Graph Neural Networks and Ensemble Learning for Mineral Prospectivity Mapping Using Geochemical Data

Kholod M. Alzubidi[1], Alaa O. Khadidos[2], Adil O. Khadidos[3], Haitham M. Baggazi[4], Fahad M. Alharbi[5], Razan Alamoudi[6]

Faculty of Computing and Information Technology-Department of Information Systems, King Abdulaziz University, Jeddah, Saudi Arabia[1, 2]

Center of Research Excellence in Artificial Intelligence and Data Science, King Abdulaziz University, Jeddah, Saudi Arabia[2]

Faculty of Computing and Information Technology-Department of Information Technology, King Abdulaziz University, Jeddah, Saudi Arabia[3]

Department of Structural Geology and Remote Sensing, King Abdulaziz University, Jeddah, Saudi Arabia[4]

Regional Geological Program, Saudi Geological Survey, Jeddah, Saudi Arabia[4, 5, 6]

***Abstract*—Mineral exploration is inherently challenging because geological formations are complex and geochemical relationships are often nonlinear and spatially variable. Although artificial intelligence has recently shown strong potential in improving mineral potential mapping, many existing approaches struggle to fully capture spatial relationships within geochemical data. In this study, an integrated framework that combines Graph Neural Networks (GNNs), ensemble learning classifiers, and unsupervised K-means clustering was developed to analyze geochemical data from Saudi Arabia. The geochemical samples were modeled as a spatial graph, where each node represents a sampling location, and the connections between nodes reflect their geographic proximity. This structure allows the GNN to better capture spatial relationships within the data, while ensemble models serve as baseline methods for performance comparison. K-means clustering was further used to examine spatial patterns and highlight potential mineralization zones. The proposed approach achieved strong predictive results, with classification accuracies reaching 85.08% for lithium and 90.62% for tungsten, alongside comparable performance for other elements. Overall, these results demonstrate the value of incorporating spatially-aware artificial intelligence techniques to support more accurate mineral exploration and more informed resource management.**

***Keywords*—Rare mineral mapping; geochemical data; geospatial analysis; GNN; ensemble learning**

I. Introduction

Minerals are one of the most important natural resources, helping to pay for and support economic and industrial growth. Mineral extraction and mining are closely related to progress in both technology and society. Mining has been going on in the Arabian Peninsula for more than 900 years BC, which shows that this is a long-standing activity [1].

Modern society depends on the extraction of mineral resources, which yield several valuable resources for the environment, energy, agriculture, and economics. A policy that encourages sustainable production methods is required, even though it is crucial to make sure that these resources are used responsibly [2]. Evaluating the extraction process's effects on the environment and the possibility of long-term environmental economics are key components of sustainable resource extraction.

KSA is renowned for having significant mineral resources, which might improve the economy by effectively managing and extracting rare minerals like tungsten, Li, and Rb. However, because of the extent of the country's terrain, it has historically been difficult to explore for and identify these valuable minerals [3]. Traditional methods of mineral identification require considerable time and energy, as well as the use of expensive and specialized equipment, to get the necessary data to ensure the accuracy of identification.

Geochemical surveys produce a significant amount of coherent and frequently machine-readable data. This data serves as a fundamental input for various downstream applications, including mapping, resource modeling, environmental monitoring, and assessing Mineral prospectivity [4]. Generation of geochemical examination data begins with examination design, which aims to ensure data coverage against promising areas, if any, but also depends on the setting and extent of the survey, and creates a spatial distribution of locations to be tested to maximize the probability of geological information gathering [5].

Traditional methods require significant time, power, and resources to identify minerals and sometimes require expensive, specialized equipment to achieve accuracy based on the type of mineral involved. However, early experiments have demonstrated the need for AI to contribute to mineral identification and extraction [6]. In mining and mineral exploration, AI techniques have recently produced encouraging outcomes [7]. Therefore, it is essential for mineral identification, exploration, separation, and the protection of objects in archeology by using AI [8]. Early experiments demonstrated AI's potential to contribute to intelligent minerals identification, though widespread adoption was initially limited due to computational constraints and the scarcity of labeled geochemical datasets [9].

This study focuses on applying AI models to predict the existence of rare minerals in different regions of Saudi Arabia by using the geochemical data collected from the SGC based on the concentration rates in rocks along specified latitudes and longitudes. After calculating the threshold and determining the element concentration label, the presence of the elements was predicted, with nodes identifying the geographical locations using GNN.

The main motivations behind this study are the pressing need for more efficient and scalable mineral exploration methods in KSA, given the country's Vision 2030 goals. The lack of spatially-aware AI frameworks applied to the diverse rare mineral deposits across the Arabian geological terrain. The opportunity to demonstrate that graph-based deep learning can outperform traditional tabular classifiers when spatial relationships are key. The principal contributions are:

1) A graph-based geochemical representation modeling sampling sites as nodes and geographic proximity as edges.

2) A comparative framework benchmarking GNNs against ensemble methods across eight mineral elements.

3) Integration of K-means clustering to identify mineral-rich zones without labeled data; and (d) the first multi-mineral, multi-region AI study on SGS geochemical data in Saudi Arabia.

Furthermore, the predictions were conducted based on region labeling, with data provided for ten different regions in the Kingdom, including Aban Al Ahmar, Nuqrah, Afif, etc., allowing for an effective evaluation of geographical mineral distribution patterns and resource optimization.

The proposed framework lies in three aspects: First, unlike existing studies that apply GNNs or ensemble methods independently, this work combines them in a unified pipeline where GNNs capture spatial dependencies between geochemical sampling locations, and ensemble models provide robust classification baselines for comparison. Second, the spatial graph construction, where nodes represent sampling locations and edges encode geographic proximity, is specifically tailored to geochemical data in Saudi Arabia, a domain largely unexplored using graph-based learning. Third, the simultaneous prediction of ten strategic minerals (Li, Rb, Cs, Be, Ta, Nb, Sn, W) across ten distinct regions within KSA represents a broader scope than prior studies, which typically focused on a single mineral type or non-Arabian geological contexts.

The remaining section of this study is divided into five: Section II is the literature review. Section III discusses the methodology. Section IV presents the outcomes and findings. Section V presents the discussion. Section VI covers concluding remarks.

II. Literature Review

Recent advances in AI have significantly transformed mineral prospectivity mapping by enabling data-driven modeling of complex geochemical and geological relationships. Traditional machine learning approaches, including RF, SVM, and boosting-based models, have been widely adopted to predict mineral occurrences and delineate prospective zones from multivariate geochemical datasets [4]. These models have demonstrated improved prediction accuracy compared to conventional knowledge-driven and statistical methods, particularly when applied to large-scale regional surveys [8], [9]. For instance, A. Zeb et al. utilized multivariate time series data collected over 236 days from a real gold processing plant, augmented with simulated data, at 5-minute intervals [10]. The data was acquired through the process instrumentation and control system and a digital twin platform. The modeling workflow followed the cross-industry standard process for the data mining approach, with the Spearman correlation coefficient to assess the association between features. LSTM, GRU, and CNN architectures were used. CNN recorded 36% for the average error of RMSE, 45% for MAE, and 35% for MAPE.

Furthermore, another study used satellite sensing data for predictive minerals such as copper (Cu) in Pakistan's northern region [11]. Their approaches involved geospatial data from various geoscience data sources and applied CNN, RF, and SVM models. The models were trained using 22 known Cu deposits as positive samples and an equal number of non-deposit locations selected based on point pattern analysis. The CNN model recorded high accuracy in predicting the Cu deposits, while the RF was deemed the best result for exploration, reaching an AUC greater than 0.95.

D. Hu et al [12], applied the random forest model for mineral resource prediction based on geological data. This approach can indeed be applied to forecast the presence of rare minerals in regions like Saudi Arabia. The data was analyzed by upgrading five mineral models using the random forest algorithm, achieving a model accuracy of up to 95.8%. The study emphasizes the higher prediction accuracy and shorter prediction time of the random forest model. In addition, T. Sun et al, [13] was conducted in southern Jiangxi Province, China, a major global tungsten production hub with extensive geological data, rendering it ideal for training prospectivity models. It used 118 known W occurrences and eight evidential layers that came from different sources of geoscience information about W mineralization. They employed a grid search to identify the optimal parameter configurations for the ML models, subsequently evaluating them using 10-fold cross-validation. To mitigate the effects of false negatives, three datasets of non-occurrence were created. The CNN model exhibited the highest classification performance, achieving an accuracy of 92.38%.

The study [14] applied mobile computer learning and geological semantic models to predict mineralization prospects, which can be applied to existing geological data in a four-element combination to forecast rare minerals. A collection of geological attributes and a collection of examples, which are represented by GDO, GDR, GDP, and GDI. The data was analyzed by constructing a geological semantic model, utilizing a semantic knowledge library for associative search, and applying the random forest algorithm to predict mineralization prospects. The geological semantic model constructed achieved an accuracy rate of 87.9% and a recall rate of 96.5%.

S. E. Zhang et al., [15] applied ML to multivariate geochemical data from different regions in the Churchill province of Canada. ML was used to predict modern and higher-dimensional multi-elemental concentrations using existing legacy data, thereby reducing the latency for downstream

applications like prospectivity mapping. The study demonstrated the feasibility of using ML to predict elemental concentrations in areas of geochemical data.

H.-X. Liu et al., [16] used a small set of sintering data from more than a dozen W(Mo) alloys, including both solid and liquid phase sintering. This study used simple descriptors and machine learning methods like Lasso regression, k-NN, random forest, and MLP to guess the density of the sintered material. The MLP achieved predictions ($R > 0.950$), and the difference between the predicted and experimental values was less than 0.063, which indicates that the model is useful.

L. Ding et al, [17] proposed an AI model named Geo-Meta to predict multiple geological samples. Geo-Meta applied fusion features and computed prototypes in the metric space, which incorporated a semi-supervised model based on label propagation and quantified the similarity between sample features. Their model achieved an AUC of 98% without data augmentation and an accuracy of 93% for ore deposits within only 7% of the study area. The results provided valuable technical support for decision-making in target area exploration. But the limitation was in the imbalanced sample size of the study, 351 of which were positive and 10,472 of which were negative.

C. Li et al., [18] designed a multi-scale CNN-Transformer model for minerals mapping in the region of the Southern Xing'an. The data collection included 14 geochemical elements, stratigraphy, rock bodies, geological structures, and aeromagnetic data. While Transformers were capturing global relationships and long-range dependencies, they combined a multi-scale CNN-Transformer with a CNN to extract local features. Their model's mineral prospectivity mapping accuracy was 0.92%.

R. Tan et al, [19] proposed an ML model to classify mineral deposits using sphalerite chemistry and associated mineral assemblages. The model utilizes sphalerite trace-element chemistry (12 elements) and associated minerals assemblages (15 minerals) collected from 3159 sphalerite analyses across 109 ore deposits worldwide. Mineral assemblage data are parameterized as binary (0 for absence, 1 for presence). The study employs a composite ML model consisting of two sub-models: Random Forest (RF) for trace-element data and Extra Random Trees (ERT) for minerals assemblage data, and the SHAP method for feature importance. The composite model achieved a high accuracy of $85 \pm 1.4\%$ and an AUC of 0.93 ± 0.01. M. Radulescu et al., [20] demonstrated the application of quantized deep learning, specifically using the popular EfficientDet architecture, in the context of mineral identification during mining. The authors propose a post-training quantization method for the EfficientDet model that reduces its size and complexity while maintaining performance. Using a custom minerals dataset, the quantization was tested using 8-bit symmetric quantization, and the effectiveness of the model was assessed by contrasting the quantized version with the original floating-point model. On the given dataset, the pre-trained EfficientDet model showed a precision of 0.78 and a recall of 0.65. The quantized model, on the other hand, demonstrated a notable improvement, attaining 0.80 recall and 0.88 accuracy. The accuracy of the suggested model was a remarkable 90.5%.

The use of AI for minerals exploration and geostatistical modeling has advanced significantly, according to an analysis of earlier research. Many works have used AI and machine learning to efficiently predict and assess mineral resources across a variety of datasets and geographical regions. These studies have explored single-element analysis as well as multi-element datasets, with some utilizing geospatial imagery for geological surveys.

According to the analytical review of prior studies, the majority of them concentrated on a single rare mineral or a small number of them, using some models, such as CNN, RF, and SVM, to predict mineral occurrences and classify deposits. In addition, some studies used geospatial data in geochemical exploration with imagery to predict multi-element concentrations or mineralization potential.

However, the gap lies in the limited geographical scope and mineral diversity in existing studies. In contrast, the current study addresses rare gaps by analyzing ten essential and strategic minerals across various regions in the KSA. This is one of the first studies to cover such a broad spectrum of rare minerals, with a geospatial analysis considering latitude and longitude coordinates for the different regions in KSA.

III. Methodology

In the Method section, the dataset from the Saudi Geological Survey (SGS) includes detailed geochemical information on rare minerals such as lithium and rubidium. It also contains trace metal concentrations in collected rock samples. The method begins with data collection and analysis of rock samples from ten different regions of Saudi Arabia. The dataset is preprocessed to normalize values and address nulls or missing data. It is then split for training and validation, taking into account factors such as longitude and latitude. ML models, including Graph Neural Network (GNN), XGBOOST, RF, and K-Means Cluster, are used to predict mineral presence and analyze regional trends. Fig. 1 shows the overview of the steps and proposal models in predicting the rare mineral concentrations in KSA. After data preprocessing and threshold-based labeling, three complementary learning strategies are applied in parallel. A GNN captures spatial dependencies through graph-based learning, ensemble models provide robust tabular classification baselines, and clustering identifies mineral-rich zones in an unsupervised manner. The combined outputs support spatial interpretation and decision-making in mineral exploration. Nodes represent sampling locations, while elemental concentrations are treated as node features.

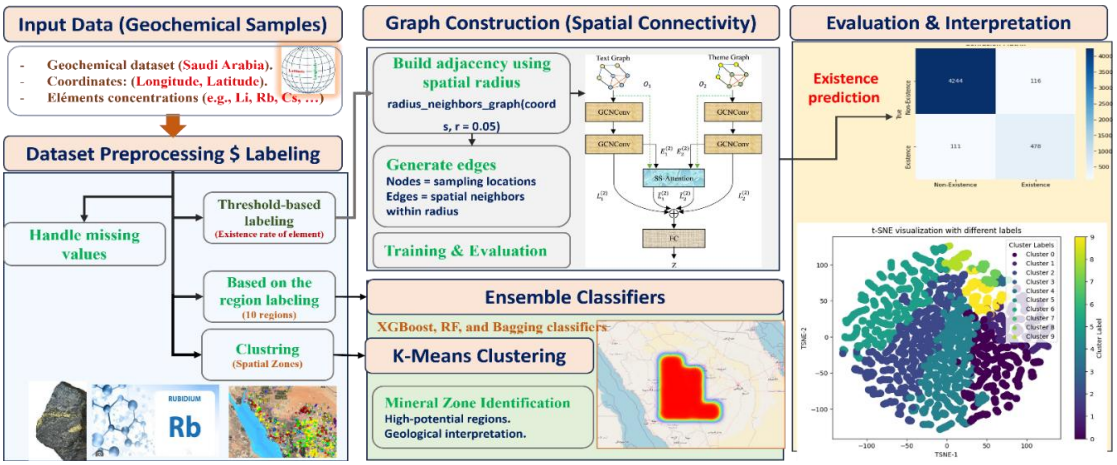

Fig. 1. The overall workflow of the proposed geochemical mineral prediction framework.

A. Data Description

The dataset was collected from the SGS, which is responsible for all specialized earth technology paintings inside the Kingdom of Saudi Arabia [21].

From the simple work on geologic mapping to the conduct of applied geoscientific studies, especially on minerals and groundwater explorations, and the development of mineral sources, along with the provision of investment opportunities within the field of mining. The SGS serves as the primary source of scientific information in Saudi Arabia, providing technical reviews, geologic maps, mineral sources, and other relevant geologic statistics throughout the Kingdom.

The Geological Survey collects data on several minerals in various regions of the Kingdom of Saudi Arabia, then analyzes their composition and mineral concentrations within the rocks. In this study, data on rare minerals such as Lithium (Li), rubidium (Rb), cesium (Cs), beryllium (Be), tantalum (Ta), niobium (Nb), tin (Sn), and tungsten (W) were extracted for 10 regions of the Kingdom, as shown in Table I. Each region contains a set of rock samples with the percentage of each mineral identified.

TABLE. I. THE ROCK SAMPLES FOR ALL RARE MINERALS ARE IN SEVERAL REGIONS OF KSA.

Region	Number of mineral samples
Aban Al Ahmar	2,428
Nuqrah	2,550
Afif	2,451
Wadi Ar Rika	2,546
Al Hissu	2,519
Mahad Adh Dhahab	2,535
Al Muwayh	2,466
Zalim	2,295
Miskah	2,415
Wadi Ash Shubah	2,538
Total	**24,743**

B. Dataset Preprocessing

The longitude and latitude of each rock sample were recorded, along with the percentage and concentration of the mineral. For example, in a sample from the Aban al-Ahmar region, lithium (Li) represented 22.9 mg/kg, and Nb represented 5.33 mg/kg. Initially, only the eight rare elements were extracted, according to the recommendations of the Geoscience Authority, from a total of 64 mineral elements for all 10 regions. They were combined into a single CSV file with the longitude and latitude coordinates. All null values are removed. The rest of the values are normalized by Min-Max scaling.Avoid combining SI and CGS units, such as current in amperes and magnetic field in oersteds. This often leads to confusion because equations do not balance dimensionally. If you must use mixed units, clearly state the units for each quantity that you use in an equation.

1) Define label (Target variable): Since the data on mineral elements has a rate of presence in rock samples, there are no binary labels. The data needs to define an explicit label as a target variable label for mineral presence.

The study proposed creating a proxy target based on known geochemical thresholds indicating the presence/absence of rare minerals. Define threshold-based labeling that identifies high concentrations of specific elements as indicators of mineralization, using the calculation of the arithmetic mean and standard deviation [22].

Mean represents the concentration of the data across all samples. The equation calculates the arithmetic mean in Eq. (1):

$$\text{Mean} = \frac{1}{N}\sum_{i=1}^{N} x_i \quad (1)$$

where, xi is the value of the i-th sample, N is the number of samples.

The Standard Deviation (σ) represents the deviation of the data from the mean, or the spread of the data points around the mean [see Eq. (2)]:

$$\sigma = \sqrt{\sqrt{\frac{1}{N}}\sum_{i=1}^{N}(x_i - \mu)^2} \quad (2)$$

where, μ is the arithmetic mean and N is the number of samples. After that, determining the range using the standard deviation by Eq. (3) is as follows [23]:

$$Range = \mu + k\sigma \quad (3)$$

where, μ is the arithmetic mean, k is the constant related to the confidence level (usually 1, 2, or 3 standard deviations), and σ is the standard deviation.

After determining the range, identify the samples that contain high concentrations, indicating the presence of the element. If the value of the sample is greater than the upper limit of the range, it indicates that a specific element is present, and if it is less than the lower limit, then the element is absent. Table II shows the threshold value for each element and the threshold-based labeling for both values, existence = 1 and non-existence = 0, after comparing the rate of concentration with the threshold value for all samples.

TABLE. II. THE THRESHOLD VALUE FOR EACH ELEMENT AND THE THRESHOLD-BASED LABEL FOR ALL ELEMENTS ARE DETERMINED AFTER COMPARING THE RATE OF CONCENTRATION TO THE THRESHOLD VALUE.

Mineral	Threshold	Rate of existence Label=1	Rate of non-existence Label=0
Li	14.23	3,211	21,532
Rb	96.62	2,956	21,787
Cs	1.90	3,026	21,717
Be	2.22	2,153	22,590
Ta	1.01	1,843	22,900
Nb	14.58	1,796	22,947
Sn	2.99	1,150	23,593
W	1.79	123	24,620

C. Dataset Splitting for Training and Testing

The dataset consists of two classifications for each mineral: existence and non-existence. The 80% - 20% splitting method is applied to each category to create training and testing datasets. Specifically, 80% of the data is used for training the model, while 20% is used for testing. Table III provides a breakdown of the number of samples for each mineral in the dataset, split into training (80%) and testing (20%) sets. For example, for Li, there are 3,211 total samples of existence, split into 2,603 for training and 608 for testing.

D. Dataset Splitting for Training and Testing based on the Region

The data on existing minerals is defined for their regions. Ten regions in KSA are recorded with the concentration rate of minerals. In this study, there is a second scenario that conducts the classification based on the region, so the dataset is prepared by the addition of a column of regions as a label. The separation of the dataset into 70%, 15%, and 15% for training, validation, and testing sets based on the region is shown in Table IV, which presents the rate for each region, such as Afif and Al Hissu.

Fig. 2 refers to the correlation matrix for latitude, longitude, and the selected rare elements. The results provide weak indications of moderate correlations between geographical variables and element concentrations and show a moderate negative correlation of R = -0.36 with longitude and latitude. Strong positive correlations between NB and TA with R = 0.96 and RB, Cs, and BE (R = 0.62–0.78) were seen, suggesting shared geochemical sources. In contrast, W showed weak correlations. The "region" variables showed a minimum effect on the distribution of the element, indicating limited spatial control over the geochemical pattern.

TABLE. III. SPLITTING THE DATASET 80%-20% FOR TRAINING AND TESTING SETS FOR EXISTENCE AND NON-EXISTENCE CLASSIFICATION.

Mineral	Rate of existence	(80% - 20%) splitting of existence	Rate of non-existence	(80% - 20%) splitting of non-existence
Li	3,211	2,603 - 608	21,532	17,191 – 4,341
Rb	2,956	2,367 - 589	21,787	17,427 – 4,360
Cs	3,026	2,446 - 580	21,717	17,348 – 4,369
Be	2,153	1,730 - 423	22,590	18,064 – 4,526
Ta	1,843	1499 - 344	22,900	18,295 - 4605
Nb	1,796	1455 - 341	22,947	18339 - 4608
Sn	1,150	930 - 220	23,593	18864 - 4729
W	123	105 - 18	24,620	19689- 4931

TABLE. IV. SPLITTING THE DATASET 70%,15%,15% FOR TRAINING, VALIDATION, AND TESTING SETS BASED ON THE REGION OF EXISTENCE OF THE MINERAL.

The region	Training set (70%)	Validation test (15%)	Testing test (15%)
Aban_Al_Ahmar	1724	344	360
Afif	1745	345	361
Al_Hissu	1776	371	372
Al_Muwayh	1749	349	368
Mahad_Dhahab	1755	387	393
Miskah	1661	384	370
Nuqrah	1759	400	391
Wadi_Ar_Rika	1762	388	396
Wadi_Shubah	1810	375	350
Zalim	1577	368	350

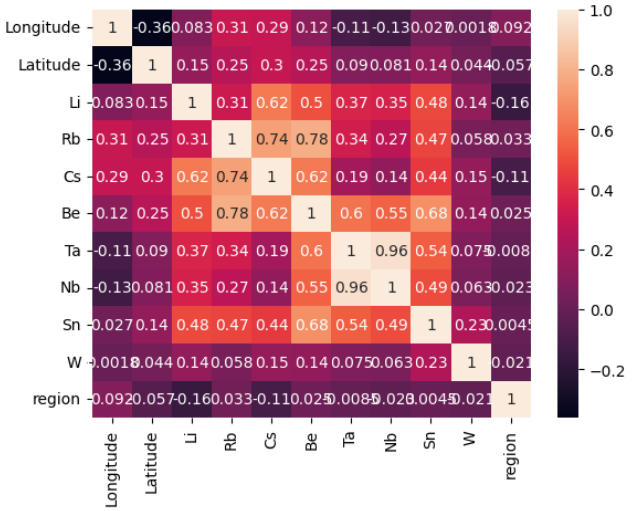

Fig. 2. The correlation matrix of the rare elements with latitude and longitude based on the region.

E. The Artificial Intelligence Models

1) GNN: Record structure along with object entities known as nodes, which are connected through a manner of relationships referred to as edges [24]. Both the nodes and edges can maintain records inside the shape of attributes, any of which may also be additionally characteristic as variables in machine learning assessment.

There is more than one type of graph neural network. One commonly used variation of the GNN algorithm is the graph convolutional network, or GCN [25]. A GCN updates records on every node by aggregating facts from neighboring nodes using a weighted sum, with the weight relying on the number of nodes connected to the recipients [26].

In this study, nodes represent the geochemical sample points, each with associated features such as elemental concentrations. Edges define the relationships between nodes, which can be based on spatial proximity or geochemical similarity. The graph is constructed using spatial proximity as the defining criterion for edges. Specifically, nodes are connected if they fall within a defined radius (e.g., 5 km). This spatial-based adjacency matrix is created using the radius_neighbors_graph function from the sklearn.neighbors module, which helps determine the connectivity between sample points based on their geographical coordinates (longitude and latitude). Fig. 3 presents the subsampled visualization of the spatial graph. Nodes represent geochemical sampling locations, and edges indicate neighborhood connections within a predefined spatial radius. The subsampling is applied for visualization clarity, while the complete spatial graph is used during model training. For visualization purposes, only a subset of nodes and edges is displayed to avoid visual clutter; however, the full graph connectivity is preserved during training. The Adam optimizer with a learning rate of 0.01 trains the model, and the loss function is cross-entropy loss with 200 trained epochs.

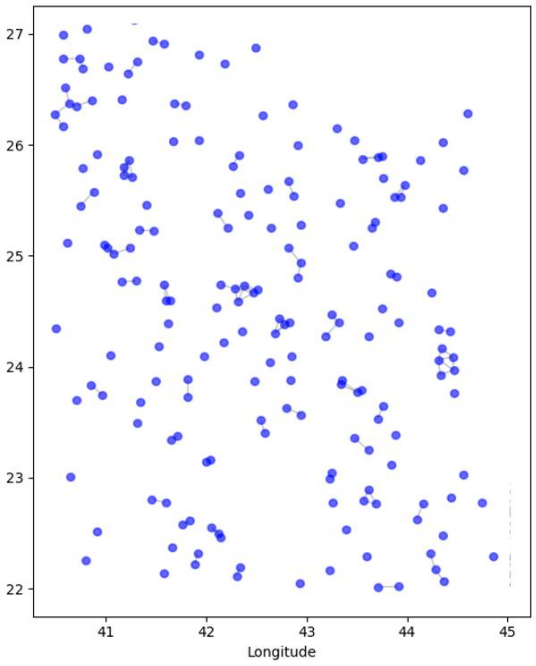

Fig. 3. Subsampled visualization of the spatial graph.

All hyperparameters were selected empirically based on preliminary experiments and kept fixed across all reported results.

2) XGBoost model: XGBoost is a tree boosting system that can grow and use a lot of new methods and algorithms to get the best results. It makes machine learning tasks very scalable [27]. These methods deal with problems like learning trees that are close to the truth, working with sparse data, and doing math quickly with large datasets [28]. This algorithm adds a default direction to each tree node. If a feature value is missing from the sparse matrix, the instance is put into this default direction. The information is used to figure out the best default directions.

3) Random forest model: The random forest, as an ensemble learning approach, was developed to combine bagging with random feature selection [27]. It describes how it constructs decision trees using bootstrap sampling and applies randomization during node splitting, often using the Gini index for feature selection. Key advantages of RF include robustness to noise, resistance to overfitting, and high accuracy [29]. Over the past decade, research has focused on boosting RF's performance through various extensions. These include methods to determine the minimum number of trees, using multiple attribute evaluation measures and weighted voting, dynamic integration techniques, and weighted random sampling for feature selection.

4) Ensemble bagging models: The bagging method is also known as bootstrap aggregating [30]. This refers to creating many little ones from most of the data in the dataset itself. The goal of bagging is to create a more diverse future match model by adjusting a stochastic distribution of training data sets, where small changes in training data sets will make significant changes to predictions [31]. In bootstrapping, the training of the ensemble models on bootstrap replicates the training dataset.

5) Unsupervised ML models (K-means clustering): In this study, we use K-means to generate the labels based on the regions that contain minerals and then compute the silhouette points for clustering. Unsupervised clustering was used for exploratory spatial analysis and then apply classification using the supervised learning models. K-means depends on the value of K, which must always be specified to analyze all clustering. Clusters with different K values will eventually produce different results [32]. Different scheme problems analyzed in recent studies did not consider the problem where the algorithm is only converted to a poor local minimum. An alternative approach was used to prevent the K-means algorithm from being easily affected by noise and external values.

F. Evaluation

Various commonly used assessment criteria, such as precision, accuracy, F1-score, and recall, are utilized to train and test the suggested models [33]. The specific mathematical definitions for each metric are as follows [see Eq. (4) to Eq. (7)]:

$$\text{Precision (Pre.)} = \frac{\text{TP}}{\text{TP+FP}}, \tag{4}$$

$$\text{Recall/Sensitivty (Se.)} = \frac{\text{TP}}{\text{TP+FN}} \tag{5}$$

$$\text{Accuracy (Acc.)} = \frac{\text{TP+TN}}{\text{TP+TN+FP+FN}} \quad (6)$$

$$\text{F1} - \text{score (F1} - \text{s.)} = \frac{2*\text{Precision}*\text{Sensitivity}}{\text{Precision+Sensitivity}} \quad (7)$$

The silhouette score method, which is a measure of the quality of a cluster, was used to find the silhouette coefficient for all samples for different clusters [34], as in Eq. (8):

$$Silhouette = \frac{1}{N}\sum_{i=1}^{N} s(i) \quad (8)$$

where, N is the total number of data points, s(i) is the Silhouette Score for point i [see Eq. (9)]:

$$s(i) = \frac{b\,(i)-a(i)}{\max\,(a(i),b(i))} \quad (9)$$

where, a(i) is the cohesion of point i within its own cluster. In other words, it is the average distance between point i and all other points in the same cluster. b(i) is the separation of point i from the nearest cluster. It is the distance between point i and the closest centroid of any other cluster.

A confusion matrix is a determinant that is used to define the general performance of a set of performances. It represents counts from predicted and actual values. The output True Negative (TN) shows the quantity of negative samples classified correctly. Similarly, True Positive (TP) indicates the variety of effective samples classified successfully. False Positive (FP), the number of real negative samples classified as highly incorrect, and False Negative (FN), which is the form of real high-quality samples labelled as negative.

The precision-recall curve for the performance of a GNN model classification, in particular for binary classification tasks, will be used. The curve is derived from the precision_recall_curve feature from sklearn metrics, which calculates precision and recall for different threshold values of predicted probabilities.

G. Experimental Setup

The experiments were performed using an MSI GS66 laptop that has the following properties: an Intel Core i7 11800H (11800H) processor, 32 GB RAM, 2 TB SSD NVMe storage, and an RTX 3080 graphic card with 16 GB memory. The experiments mentioned in this article were performed using Python 3.10 on Windows 11.

IV. Results

The primary findings from predicting the presence and distribution of rare mineral elements in various Saudi Arabian regions using various ML and AI models are presented in this section. The performance of these models is shown in the following scenarios, which start with GNN-based rare mineral prediction, move on to region-based classification using ML ensemble models, and conclude with an unsupervised learning method for locating mineral-rich clusters.

A. GNN Model to Predict the Existence of Mineral Elements

In this use case, a GNN was used to predict the existence of the rare mineral elements based on their concentrations in rock samples collected from different areas of Saudi Arabia. The performance of the models was evaluated by the common classification measures such as accuracy, precision, recall, and F1 score. The GNN model produced very high accuracy for each of the rare mineral elements, with tungsten achieving the highest accuracy at 90.62%, as shown in Table V. However, there has been a variance in precision and recall. For example, lithium and tin had decreasing recall scores, indicating that the model missed some of their occurrences, whereas rubidium and niobium demonstrated a fair mix of precision and recall.

TABLE. V. Predicting the Performance of the Existence of Rare Mineral Elements using a GNN Model.

Mineral	Accuracy	Precision	Recall	F1 Score
Li	85.08	68.31	64.42	66.09
Rb	86.41	71.19	72.34	72.82
Cs	86.11	71.40	68.07	69.70
Be	87.00	71.00	61.92	66.19
Ta	88.01	68.68	70.94	69.80
Nb	88.33	72.57	70.18	71.36
Sn	88.49	71.77	48.27	58.02
W	90.62	47.06	44.44	45.71

The findings verified that Li had an 85.08% accuracy rate, meaning the model performed well in predicting whether lithium would be present in the rock samples. Nevertheless, the recall only reached 64.42%, indicating that some lithium cases were missed by the model. The Rb element, on the other hand, had a moderate balance between accuracy and recall, as indicated by its F1 score of 72.82% in Table V. This proves that there are few false positives or false negatives and that the model is successful in identifying samples that contain rubidium.

As a common assessment of the GNN model, it achieved robust results in predicting the presence of mineral elements based on geochemical records, especially in terms of overall accuracy. However, further development is needed to address the recall issues of specific minerals, such as tin and tungsten, by using more samples or applying data augmentation, which would improve the overall performance of the model.

Fig. 4 includes multiple precision-recall curves (one for each class or feature), indicated by the labels Nb, Sn, W, etc. Each subplot visualizes the relationship between precision and recalls for a different variable or class in the dataset: Nb, Sn, W, etc., likely represent different categories or features in the data, showing how well the model performs across multiple aspects of the classification task. The variations between subplots might suggest that some classes (like W) have a poorer precision-recall trade-off, indicating possible issues with the model's ability to classify those instances accurately. Conversely, classes like Nb and Sn might show better balance, where precision and recall are relatively stable.

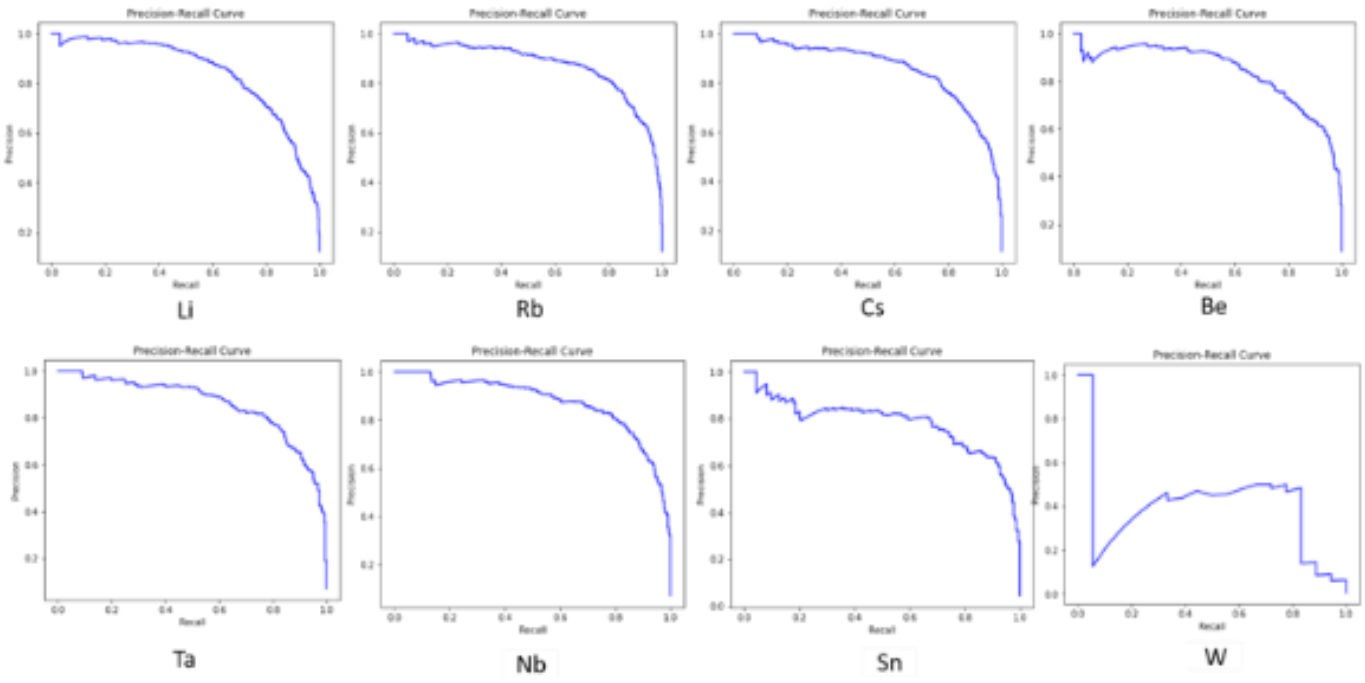

Fig. 4. The precision-recall curve of the GNN model for all the mental rare elements prediction.

The GeoPandas library in Python was used to load and plot a geographic map of Saudi Arabia from a Shapefile, which was downloaded from the Natural Earth website (https://www.Naturalearthdata.Com/downloads/10m-cultural-vectors).

Once the map is plotted, the attention of elements is concentrated by extracting the coordinates of longitude and latitude from the data, as shown in Fig. 5(a). The heatmap generated using Folium visualizes the geographic distribution of the data points based on their latitude and longitude values, as shown in Fig. 5(b).

The intense red areas suggest areas with an excessive concentration of data points, even as the cooler blue tones constitute areas with fewer occurrences. This visualization gives a clean evaluation of spatial styles, highlighting areas of extensive pastime or interest. The significant area, as shown, features a high density of elements, which may also correspond to a key location of attention in the dataset. Whilst Fig. 5(c) focuses on the centration for the Aban Alahmer region.

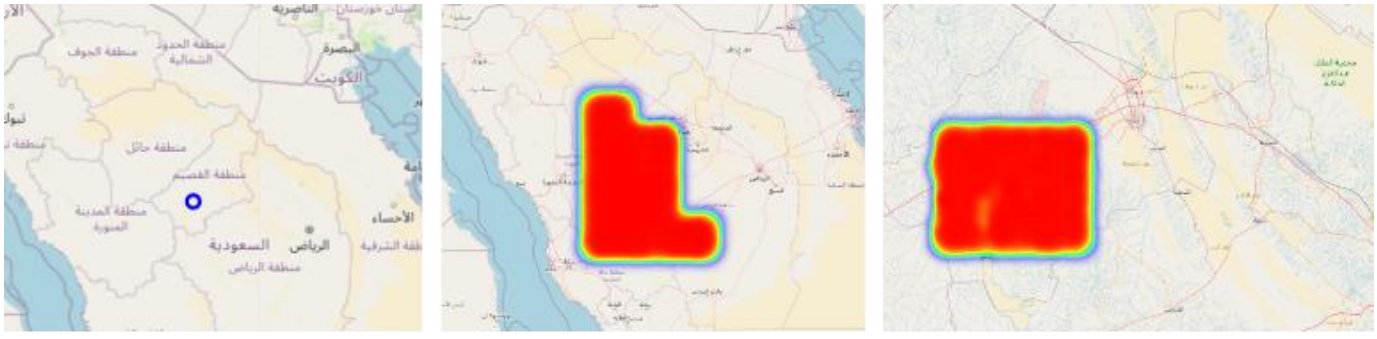

Fig. 5. A high-density concentration of element features in different regions: (a) KSA map, (b) all ten regions, and (c) Aban Alahmer.

B. The Performance Results of AI Ensemble Models to Classify based on the Region in KSA

In this use case, the regional-based classification performance results, the ML and ensemble models have shown remarkable accuracy and efficiency. Table VI presents the performance of three ML models used for region-based classification.

TABLE. VI. THE PERFORMANCE RESULT OF THE ML AND ENSEMBLE MODELS IN PREDICTING BASED ON REGION CLASSIFICATION.

Model	Accuracy	Precision	Recall	F1 Score
Xgboost	90.25	90.23	90.25	90.24
RF	89.90	89.93	89.89	89.90
BaggingClassifier	90.62	90.63	90.64	90.62

The XGBOOST model achieved an accuracy of 90.25%, a precision of 90.23%, a recall of 90.25%, and an F1 score of 90.24%. The model also performed an AUC score of 90.58%, indicating a strong ability to distinguish between different classes.

For the RF model, the model achieved an accuracy of 89.90%, a precision of 89.93%, a recall of 89.89%, and an F1 score of 89.90%. While the AUC point for RF was 90.39%, which indicates its specific performance in classification functions. However, BaggingClassifier improved both XGBOOST and RF when it comes to all performance matrices. It achieved the highest accuracy of 90.62%, with the precision, recall, and F1 scores of 90.63%, 90.64%, and 90.62%, respectively. The bagging classifier also achieved the highest AUC point of 90.69% and strengthened its position as the most effective model compared to the others.

Fig. 6 provides the confusion matrix for the three proposed models and shows the classification performance visually. Matrices indicate real positivity, false positivity, real negativity, and the number of false negatives for each class. This visual representation confirms the high classification accuracy of the model, especially in identifying the regional classes in KSA correctly. Overall, these results show the strength and reliability of the proposed model, with a bagging classifier that appears to be the most effective model for regional classification functions in KSA.

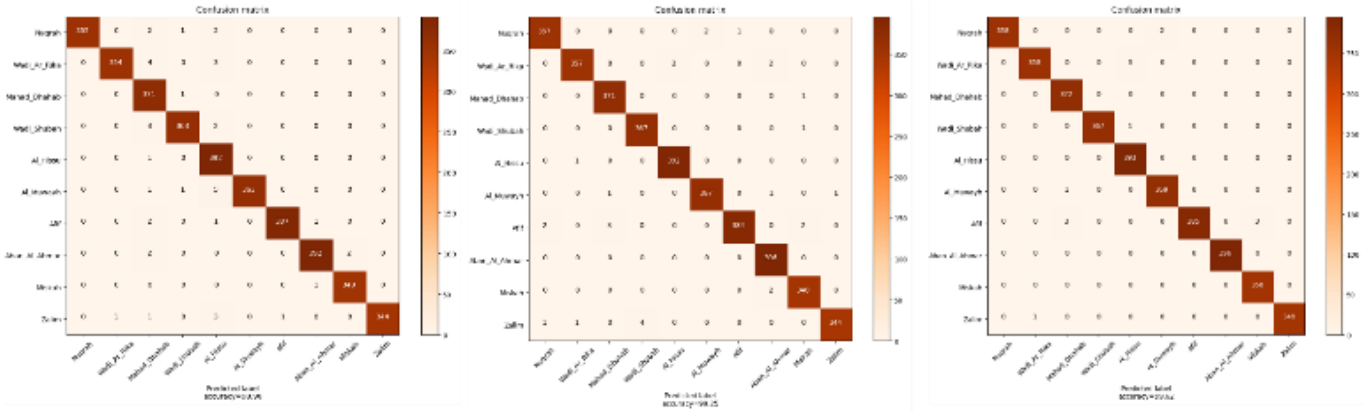

Fig. 6. The confusion matrix of the ML and ensemble models in predicting based on region classification.

C. The Performance Results of the Unsupervised AI Models

In this use case, the K-Means unsupervised learning algorithm was applied to generate rare minerals resource regions in the KSA with a cluster k=10 based on the values classified in the second scenario. The elbow library was used to determine the optimal number of clusters (k). The relationship between the number of clusters (K) and the associated inertia values is plotted in Fig. 7(a). The elbow point is three, the point at which the curve starts to slope.

It selected K=10 for this investigation because it showed a sufficient reduction in inertia while maintaining significant data point groupings. Based on the information from Scenario 2, this value of K was then used to categorize the KSA's rare mineral resource regions. To identify and target areas of interest for resource extraction or conservation, the clusters created with K=10 offer clear groupings.

The results of the cluster technique appear to be fairly good; however, it didn't achieve an optimal score. Based on a Silhouette score of 0.385, the cluster shows some separation, but there are areas of overlap of some degree or errors in the calculations. Nevertheless, the results indicate an average clustering quality rating for the first training.

In Fig. 7(b), the T-SNE visualization displays the outcomes of clustering with K = 10. Each cluster is represented by a distinct color. Examining the distribution of data points across various clusters is made simpler by the scatter plot's use of two components (TSNE-1 and TSNE-2) to reduce the original data values and display them in 2D space.

Table VII presents the performance metrics of the proposed models of ML and ensemble in predicting region classifications and representing the K-means clustering results. The XGBoost model recorded an accuracy of 90.25% and an F1 score of 90.24%. The AUC value of 90.58% further signifies the model's ability to distinguish between different classes effectively.

The RF model also performs strongly with an accuracy and recall of 89.90% and 89.89%. However, its AUC score of 90.39% indicates good discriminatory power. The Bagging Classifier outperforms the other two models, achieving the highest accuracy and F1 score among the three with 90.62%. The AUC score of 90.69% indicates that this model has the best ability to correctly classify the different regions.

TABLE. VII. THE PERFORMANCE RESULT OF THE ML AND ENSEMBLE MODELS IN PREDICTING BASED ON REGION CLASSIFICATION AND REPRESENTATION OF THE K-MEANS CLUSTERING.

Model	Accuracy	Precision	Recall	F1 Score
Xgboost	90.25	90.23	90.25	90.24
RF	89.90	89.93	89.89	89.90
BaggingClassifier	90.62	90.63	90.64	90.62

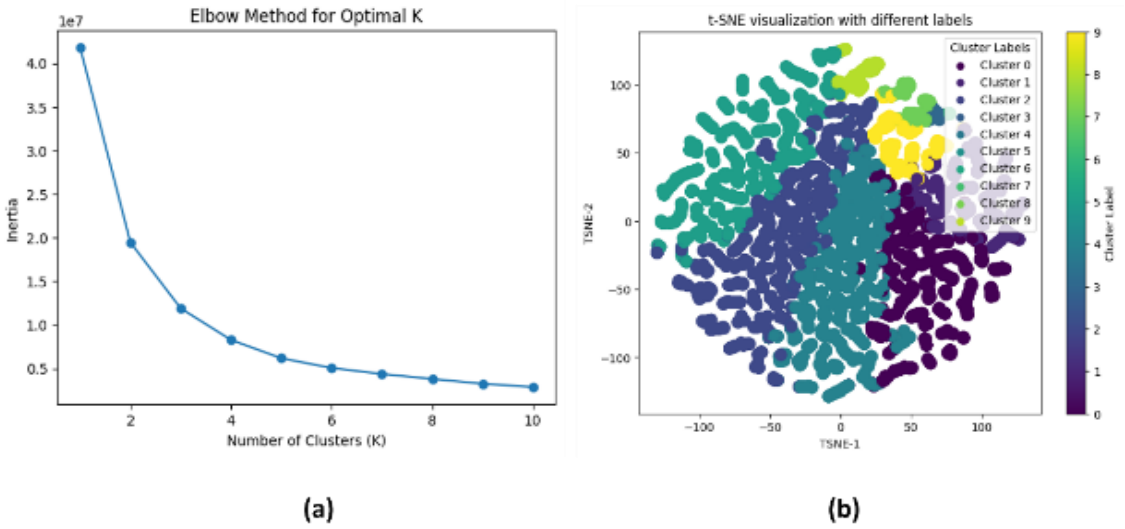

Fig. 7. The representation of the K-means clustering method based on the region: (a) Elbow curve used to select the optimal number of clusters. (b) t-SNE visualization showing the distribution of samples across the resulting clusters.

V. Discussion

The results obtained in this study demonstrate the effectiveness of integrating graph-based deep learning with ensemble methods for mineral prospectivity mapping in Saudi Arabia. This section interprets the key findings, discusses their implications, and situates them within the broader context of related literature.

A. GNN Performance and Spatial Learning

The GNN model achieved competitive classification accuracy across all eight rare mineral elements, with tungsten (W) reaching the highest accuracy at 90.62% and lithium (Li) at 85.08%. These results confirm that modeling geochemical sampling locations as a spatial graph, where edges encode geographic proximity, enables the network to exploit spatial dependencies that are invisible to conventional tabular classifiers. However, the recall limitations observed for tin (Sn, 48.27%) and tungsten (W, 44.44%) suggest that class imbalance in the geochemical dataset remains a challenge. These elements have fewer confirmed occurrences in the sampled regions, which reduces the model's ability to identify all positive cases. Future work could address this through data augmentation strategies or oversampling techniques such as SMOTE, as is effective in similar geoscience classification tasks.

B. Ensemble Models and Regional Classification

In the region-based classification scenario, all three ensemble models, XGBoost, Random Forest, and BaggingClassifier, achieved accuracies exceeding 89.9%, with BaggingClassifier performing best at 90.62%. This strong performance across all metrics (precision, recall, F1, and AUC) indicates that the regional geochemical signatures in the SGS dataset are sufficiently discriminative for automated classification.

Ensemble models match or slightly outperform the GNN in regional classification, as this task depends more on feature distributions than spatial relationships. This highlights their complementary strengths: GNNs excel with spatial structure, while ensemble methods remain highly effective for tabular data.

C. Evaluation of Comparisons Related to Recent Research Results

This section compares the performance of various AI algorithms applied to different metasearch exploration datasets, as shown in Table VIII. Studies have utilized a wide range of data sources, including time series from gold processing plants, remote sensing data for copper ore, and geological datasets from multiple regions such as China, Pakistan, and Saudi Arabia.

TABLE. VIII. Comparison of previous Studies Related to Mineral Resource Prediction.

Reference	Dataset used	AI models	Performance
[10]	Data from a gold processing plant (236 days, time series data)	LSTM, GRU, CNN	CNN: RMSE 36%, MAE 45%, MAPE 35%
[11]	Remote sensing data for copper ore in North Waziristan, Pakistan	CNN, RF, SVM	CNN: High accuracy, RF: AUC > 0.95
[13]	Geological data from Jiangxi Province, China	CNN	CNN: 92.38% accuracy, RF: 87.62%
[12]	Geological data for regions in Saudi Arabia	Random Forest	95.8% accuracy in predicting mineral presence
[15]	Multivariate geochemical data from Canada	ML (various algorithms)	Prediction of elemental concentrations using legacy data
[16]	Small dataset of sintering data for W(Mo) alloys	Lasso Regression, k-NN, Random Forest, MLP	High prediction accuracy for sintered density (R > 0.950)
Current study	Saudi Geological Survey (SGS)	GNN and Ensemble bagging models	90.62 for W mineral, and 90,69%

D. Limitations and Future Work

Despite the promising results, several limitations should be acknowledged. First, the dataset is limited to ten regions and may not generalize to unexplored areas of KSA with different geological characteristics. Second, the GNN's recall performance for certain elements indicates room for improvement, particularly through more balanced training data. Third, the current graph construction relies solely on geographic proximity; future work could explore incorporating geological similarity or geochemical correlation as additional edge-weighting criteria to further enhance the spatial representation. Extending the framework to incorporate remote sensing data, 3D geological models, and modern models such as federated learning [35].

VI. Conclusion

In the provided study, AI techniques were effectively leveraged to predict the presence of rare minerals in rock samples from the KSA. ML models, such as GNN, XGBoost, RF, and ensemble bagging models, analyze geochemical data from more than 24,000 samples in many regions in KSA. This study showed the feasibility of applying AI for the exploration of rare minerals and resource management in geological investigations containing mineral concentration data.

The performance recorded improved prediction results in all models, especially with the ensemble bagging classifier, which improved others with an outstanding accuracy of 90.62%. GNN models, while strong in general accuracy, showed the significance of fine-tuning recall values, particularly for elements like tin and tungsten, to improve the model's accuracy.

These outcomes demonstrated how well the ML model performs in handling intricate geospatial difficulties and forecasting the existence of valuable minerals using geochemical signatures. Furthermore, the regional distribution patterns of rare minerals were shown by the unsupervised approach using the K-means clustering model. The ability to identify mineral-rich regions was recorded by the k-means, providing a tool for possible resource extraction or conservation initiatives. Cluster results showed how unsupervised models can locate mineral-rich regions and provide a tool for possible resource extraction or conservation initiatives.

Acknowledgment

The authors would like to acknowledge the General Authority for Defense Development (GADD) in Saudi Arabia for funding the research through project number (GADD_2026_24_449).

The authors further acknowledge the Regional Geological Survey Program (RGP) and the Saudi Geological Survey (SGS).

References

[1] S. W. Merkel, "Evidence for the widespread use of dry silver ore in the Early Islamic period and its implications for the history of silver metallurgy," J. Archaeol. Sci., vol. 135, p. 105478, Nov. 2021, doi: 10.1016/j.jas.2021.105478.

[2] T. Henckens, "Scarce mineral resources: Extraction, consumption and limits of sustainability," Resour. Conserv. Recycl., vol. 169, p. 105511, Jun. 2021, doi: 10.1016/j.resconrec.2021.105511.

[3] M. S. Islam, M. M. Islam, A. U. Rehman, M. F. Alam, and M. Tarique, "Mineral production amidst the economy of uncertainty: Response of metallic and non-metallic minerals to geopolitical turmoil in Saudi Arabia," Resour. Policy, vol. 90, p. 104824, Mar. 2024, doi: 10.1016/j.resourpol.2024.104824.

[4] Y. He et al., "A review of machine learning in geochemistry and cosmochemistry: Method improvements and applications," Appl. Geochemistry, vol. 140, p. 105273, May 2022, doi: 10.1016/j.apgeochem.2022.105273.

[5] S. E. Zhang, J. E. Bourdeau, G. T. Nwaila, M. Parsa, and Y. Ghorbani, "Denoising of Geochemical Data using Deep Learning–Implications for Regional Surveys," Nat. Resour. Res., vol. 33, no. 2, pp. 495–520, Apr. 2024, doi: 10.1007/s11053-024-10317-5.

[6] R. Zuo and Y. Xu, "Graph Deep Learning Model for Mapping Mineral Prospectivity," Math. Geosci., vol. 55, no. 1, pp. 1–21, Jan. 2023, doi: 10.1007/s11004-022-10015-z.

[7] A. G. Alsulami, A. Alharbi, U. A. Khan, A. M. Al-Hejri, S. S. Alshamrani, and J. Almotiri, "Predicting tourism growth in Saudi Arabia with machine learning models for vision 2030 perspective," Sci. Rep., vol. 16, no. 1, p. 2556, Jan. 2026, doi: 10.1038/s41598-025-32509-6.

[8] M. Jooshaki, A. Nad, and S. Michaux, "A Systematic Review on the Application of Machine Learning in Exploiting Mineralogical Data in Mining and Mineral Industry," Minerals, vol. 11, no. 8, p. 816, Jul. 2021, doi: 10.3390/min11080816.

[9] T. Long, Z. Zhou, G. Hancke, Y. Bai, and Q. Gao, "A Review of Artificial Intelligence Technologies in Mineral Identification: Classification and Visualization," J. Sens. Actuator Networks, vol. 11, no. 3, p. 50, Aug. 2022, doi: 10.3390/jsan11030050.

[10] A. Zeb, J. Linnosmaa, M. Seppi, and O. Saarela, "Developing deep learning surrogate models for digital twins in mineral processing – A case study on data-driven multivariate multistep forecasting," Miner. Eng., vol. 216, p. 108867, Sep. 2024, doi: 10.1016/j.mineng.2024.108867.

[11] M. A. Mahboob, T. Celik, and B. Genc, "Predictive modelling of mineral prospectivity using satellite remote sensing and machine learning algorithms," Remote Sens. Appl. Soc. Environ., vol. 36, p. 101316, Nov. 2024, doi: 10.1016/j.rsase.2024.101316.

[12] D. Hu, H. Li, Q. Zhang, and C. Yang, "Construction of a Three-dimensional Geological and Mineral Resource Prediction Model Based on Machine Learning Algorithms," in 2023 IEEE 15th International Conference on Computational Intelligence and Communication Networks (CICN), IEEE, Dec. 2023, pp. 250–255. doi: 10.1109/CICN59264.2023.10402204.

[13] T. Sun, H. Li, K. Wu, F. Chen, Z. Zhu, and Z. Hu, "Data-Driven Predictive Modelling of Mineral Prospectivity Using Machine Learning and Deep Learning Methods: A Case Study from Southern Jiangxi Province, China," Minerals, vol. 10, no. 2, p. 102, Jan. 2020, doi: 10.3390/min10020102.

[14] Z. An, Y. Zhao, Y. Zhang, and X. Li, "Prediction of Mineralization Prospects Based on Geological Semantic Model and Mobile Computer Machine Learning," Wirel. Commun. Mob. Comput., vol. 2021, no. 1, Jan. 2021, doi: 10.1155/2021/7734080.

[15] S. E. Zhang, J. E. Bourdeau, G. T. Nwaila, and Y. Ghorbani, "Advanced geochemical exploration knowledge using machine learning: Prediction of unknown elemental concentrations and operational prioritization of Re-analysis campaigns," Artif. Intell. Geosci., vol. 3, pp. 86–100, Dec. 2022, doi: 10.1016/j.aiig.2022.10.003.

[16] H.-X. Liu et al., "Prediction of sintered density of binary W(Mo) alloys using machine learning," Rare Met., vol. 42, no. 8, pp. 2713–2724, Aug. 2023, doi: 10.1007/s12598-022-02238-0.

[17] L. Ding, B. Chen, Y. Zhu, H. Dong, and P. Zhang, "Mineral prediction based on prototype learning," Comput. Geosci., vol. 184, p. 105540, Feb. 2024, doi: 10.1016/j.cageo.2024.105540.

[18] C. Li et al., "CNN-Transformers for mineral prospectivity mapping in the Maodeng–Baiyinchagan area, Southern Great Xing'an Range," Ore Geol. Rev., vol. 167, p. 106007, Apr. 2024, doi: 10.1016/j.oregeorev.2024.106007.

[19] R. Tan, Y. Shao, M. J. Brzozowski, Y. Zheng, and Y.-Q. Xiong, "Development of a machine learning model to classify mineral deposits

using sphalerite chemistry and mineral assemblages," Ore Geol. Rev., vol. 169, p. 106076, Jun. 2024, doi: 10.1016/j.oregeorev.2024.106076.

[20] M. Radulescu, S. Dalal, U. K. Lilhore, and S. Saimiya, "Optimizing mineral identification for sustainable resource extraction through hybrid deep learning enabled FinTech model," Resour. Policy, vol. 89, p. 104692, Feb. 2024, doi: 10.1016/j.resourpol.2024.104692.

[21] S. G. S. (SGS), "Digital data and information." [Online]. Available: https://sgs.gov.sa/en/services/digital-data-and-information/types

[22] G. Smith, Standard Deviations: Flawed Assumptions, Tortured Data, and Other Ways to Lie with Statistics. ABRAMS Pres, 2022. [Online]. Available: https://books.google.co.in/books?id=_xKEDwAAQBAJ

[23] R. Usamentiaga, D. G. Lema, O. D. Pedrayes, and D. F. Garcia, "Automated Surface Defect Detection in Metals: A Comparative Review of Object Detection and Semantic Segmentation Using Deep Learning," IEEE Trans. Ind. Appl., vol. 58, no. 3, pp. 4203–4213, May 2022, doi: 10.1109/TIA.2022.3151560.

[24] J. Zhou et al., "Graph neural networks: A review of methods and applications," AI Open, vol. 1, pp. 57–81, 2020, doi: 10.1016/j.aiopen.2021.01.001.

[25] T. Kipf, "emi-supervised classification with graph convolutional networks," arXiv Prepr., no. arXiv:1609.02907, 2016, doi: 10.48550/arXiv.1609.02907.

[26] F. M. H. Sihombing, R. M. Palin, H. S. R. Hughes, and L. J. Robb, "Improved mineral prospectivity mapping using graph neural networks," Ore Geol. Rev., vol. 172, p. 106215, Sep. 2024, doi: 10.1016/j.oregeorev.2024.106215.

[27] K. H. Alnafesh, A. M. Al-Hejri, and P. Dr Sudhir Jagtap, "Exploring the Potential of Ensemble and XAI for Effective IoT Multiclass Malware Detection," in 2025 4th International Conference on Automation, Computing and Renewable Systems (ICACRS), IEEE, Dec. 2025, pp. 149–155. doi: 10.1109/ICACRS67045.2025.11324159.

[28] T. Chen and C. Guestrin, "XGBoost," in Proceedings of the 22nd ACM SIGKDD International Conference on Knowledge Discovery and Data Mining, New York, NY, USA: ACM, Aug. 2016, pp. 785–794. doi: 10.1145/2939672.2939785.

[29] K. Fawagreh, M. M. Gaber, and E. Elyan, "Random forests: from early developments to recent advancements," Syst. Sci. Control Eng., vol. 2, no. 1, pp. 602–609, Dec. 2014, doi: 10.1080/21642583.2014.956265.

[30] A. Mohammed and R. Kora, "A comprehensive review on ensemble deep learning: Opportunities and challenges," J. King Saud Univ. - Comput. Inf. Sci., vol. 35, no. 2, pp. 757–774, Feb. 2023, doi: 10.1016/j.jksuci.2023.01.014.

[31] M. R. Al-Maamari, R. Ramteke, A. M. Al-Hejri, and S. S. Alshamrani, "Integrating CNN and transformer architectures for superior Arabic printed and handwriting characters classification," Sci. Rep., vol. 15, no. 1, p. 29936, Aug. 2025, doi: 10.1038/s41598-025-12045-z.

[32] M. Ahmed, R. Seraj, and S. M. S. Islam, "The k-means Algorithm: A Comprehensive Survey and Performance Evaluation," Electronics, vol. 9, no. 8, p. 1295, Aug. 2020, doi: 10.3390/electronics9081295.

[33] A. M. Al-Hejri, R. M. Al-Tam, A. H. Sable, B. Almuhaya, S. S. Alshamrani, and K. M. Alshmrany, "A hybrid vision transformer with ensemble CNN framework for cervical cancer diagnosis," BMC Med. Inform. Decis. Mak., vol. 25, no. 1, p. 411, Nov. 2025, doi: 10.1186/s12911-025-03250-x.

[34] V. and others Pedregosa, Fabian and Varoquaux, Ga {\"e}l and Gramfort, Alexandre and Michel, Vincent and Thirion, Bertrand and Grisel, Olivier and Blondel, Mathieu and Prettenhofer, Peter and Weiss, Ron and Dubourg, "Scikit-learn: Machine learning in Python," J. Mach. Learn. Res., vol. 12, pp. 2825--2830, 2011.

[35] A. M. Al-Hejri et al., "A hybrid explainable federated-based vision transformer framework for breast cancer prediction via risk factors," Sci. Rep., vol. 15, no. 1, p. 18453, May 2025, doi: 10.1038/s41598-025-96527-0.